Climate Change and the Middle Atmosphere. Part III: The Doubled CO_2 Climate Revisited

D. RIND

Institute for Space Studies, NASA/Goddard Space Flight Center, New York, New York

D. SHINDELL

Center for Climate Systems Research, Columbia University, New York, New York

P. LONERGAN

Scientific Systems and Analysis, Inc., New York, New York

N. K. BALACHANDRAN

Center for Climate Systems Research, Columbia University, New York, New York

(Manuscript received 5 November 1996, in final form 14 July 1997)

ABSTRACT

The response of the troposphere–stratosphere system to doubled atmospheric CO_2 is investigated in a series of experiments in which sea surface temperatures are allowed to adjust to radiation imbalances. The Goddard Institute for Space Studies (GISS) Global Climate Middle Atmosphere Model (GCMAM) warms by 5.1°C at the surface while the stratosphere cools by up to 10°C. When ozone is allowed to respond photochemically, the stratospheric cooling is reduced by 20%, with little effect in the troposphere. Planetary wave energy increases in the stratosphere, producing dynamical warming at high latitudes, in agreement with previous GCMAM doubled CO_2 simulations; the effect is due to increased tropospheric generation and altered refraction, both strongly influenced by the magnitude of warming in the model's tropical upper troposphere. This warming also results in stronger zonal winds in the lower stratosphere, which appears to reduce stratospheric planetary wave 2 energy and stratospheric warming events. The dynamical changes in the lower stratosphere are weakened when O_3 chemistry on polar stratospheric cloud effects are included at current stratospheric chlorine levels. Comparison with the nine-level version of the GISS GCM with a top at 10 mb shows that both the stratospheric and tropospheric dynamical responses are different. The tropospheric effect is mostly a function of the vertical resolution in the troposphere; finer vertical resolution leads to increased latent heat release in the warmer climate, greater zonal available potential energy increase, and greater planetary longwave energy and energy transports. The increase in planetary longwave energy and residual circulation in the stratosphere is reproduced when the model top is lifted from 30 to 50 km, which also affects upper-tropospheric stability, convection and cloud cover, and climate sensitivity.

1. Introduction

Increasing attention is being paid to the coupling between different levels of the atmosphere, both in promoting short-term interannual variability and for longer-term climate change. Direct stratospheric influence on climate has been ascribed to changes in stratospheric species concentrations, such as volcanic aerosols and lower-stratospheric ozone, due to their radiative forcing. Stratospheric equilibration is important even for gases with primarily tropospheric climate forcing; because of the stratosphere's rapid radiative response time, the global warming potential of various gases is routinely calculated taking into consideration stratospheric adjustment (e.g., IPCC 1996).

Dynamical forcing of the troposphere associated with stratospheric changes is a more subtle phenomenon. Kodera (1994) noted that the change in latitudinal temperature gradient that occurs with volcanic warming of the tropical lower stratosphere could result in altered jet stream location, planetary wave propagation, and position of tropospheric troughs and ridges. Rind et al. (1992) related lower-stratospheric volcanic warming to a reduction in the tropospheric Hadley circulation. Rind and Balachandran (1995) found that quasi-biennial os-

Corresponding author address: Dr. David Rind, NASA/Goddard Institute for Space Studies, 2880 Broadway, New York, NY 10025. E-mail: cddhr@nasagiss.giss.nasa.gov

cillation (QBO) and UV variations impacted the troposphere in the Goddard Institute for Space Studies (GISS) Global Climate Middle Atmosphere Model (GCMAM) by changing tropospheric planetary wave generation and propagation. Kodera and Chiba (1995) studied the possibility that stratospheric warmings impact the tropospheric circulation by altering the meridional propagation of waves in the troposphere.

Dynamical forcing of the stratosphere by the troposphere is a well-established feature of the stratospheric winter circulation. Therefore, it is not surprising that climate changes that alter the tropospheric circulation have a dynamical effect on the stratosphere as well. In the first two papers in this series (Rind et al. 1990, henceforth paper 1; Rind et al. 1992), changes in tropospheric dynamics associated with increased atmospheric CO_2 and volcanic aerosols affected planetary wave propagation into the stratosphere, and the residual circulation within the stratosphere. A similar type of effect was induced in the model by stratospheric ozone and water vapor changes (Rind and Lonergan 1995), and by QBO and UV variations (Balachandran and Rind 1995). The reactions were often quite convoluted: changes in radiative forcing affecting either the troposphere or stratosphere or both altered tropospheric dynamics, which then further altered the stratosphere (and then troposphere). The effect was to produce dynamical responses quite at variance with the direct radiative forcing and initial assumptions.

This process was clearly seen in paper 1, in which doubled atmospheric CO_2 was used in both the troposphere and stratosphere. In that study, the troposphere was forced with increased sea surface temperatures, obtained from an equilibrium simulation with the GISS nine-level GCM (Hansen et al. 1984). In the GCMAM, energy of the longest planetary waves, waves 1–3, increased in the troposphere. With greater long-wave energy propagating into the stratosphere, the stratospheric residual circulation increased by 10%–20%, and the general doubled CO_2-induced stratospheric cooling was strongly modified in the winter polar stratosphere.

In this paper, we revisit the doubled CO_2 climate by modifying the original runs in two fundamental ways: first, the sea surface temperatures are now calculated directly in the GCMAM with an ocean mixed-layer model incorporating specified ocean heat transports (e.g., Rind and Lonergan 1995). This makes the results internally consistent; we compare the features of this simulation with the previously published results to see which of the conclusions need to be changed. Second, since alterations in the stratospheric temperature due to increased CO_2 will affect stratospheric ozone, a crude parameterization of this effect is included. The parameterization relates ozone changes to in situ temperature and the overlying column ozone amount (hence incident UV radiation); this is discussed in further detail in a companion paper (Shindell et al. 1998, henceforth paper 2). The change in ozone can potentially have a direct effect on climate, due to ozone's influence on both shortwave and longwave radiation; in addition, it can alter stratospheric temperatures, which affects tropospheric–stratospheric stability. Thus this simulation incorporates an additional expected feedback to increased CO_2, with the potential to further alter the climate of both the troposphere and stratosphere. An additional experiment conducted as an offshoot of this run allowed for polar stratospheric cloud (PSC) formation, both in the control and the $2 \times CO_2$ simulation.

Another issue of concern is how much of the stratosphere has to be resolved, and what vertical resolution is needed, in doubled CO_2 climate model studies. As noted above, in the GCMAM the energy of the longest planetary waves increased in both the troposphere and stratosphere. This was not true in the GCM (nine layers, 10-mb top) from which the sea surface temperature changes were taken. The GCM also did not produce increases in the lower-stratospheric residual circulation. Hence the stratosphere and the troposphere experienced responses that depended upon which version of the model was being run.

The GCMAM has both a fully resolved stratosphere and somewhat greater vertical resolution in the troposphere–stratosphere system. Where the top of the model should be located for doubled CO_2 assessments has not been an object of scrutiny; the IPCC (1992) summary of model simulations did not even think to list the location of the various models' dynamical top (most were at 10 mb). Current models participating in the Atmospheric Model Intercomparison Experiment (AMIP) simulations generally have tops between 1 and 20 mb (Phillips 1994). The models in the IPCC (1992) assessment generally had between 9 and 12 layers in the vertical; the AMIP models generally have between 10 and 20; again there has been little systematic effort to explore the impact of differing vertical resolution, especially on climate change simulations.

Therefore, another goal of this study is to explore the differences between GCM and GCMAM simulations. Six different doubled CO_2 experiments will be used, two each with the GCM and GCMAM vertical resolution/top location, and two hybrid simulations. Effects in both the stratosphere and troposphere will be discussed.

The format of the simulations is given in section 2. The doubled CO_2 simulation with interactive sea surface temperatures, and a comparison between the GCMAM and GCM simulations, is presented in section 3. The effect of including the ozone feedback is discussed in section 4. The additional experiments incorporating a parameterization for PSCs are presented in section 5. A general discussion focusing on how the results obtained depend on various factors is given in section 6, and conclusions and a summary are given in section 7.

2. Model and experiments

The model used for the new experiments is the GISS GCMAM (Rind et al. 1988a; Rind et al. 1988b) with

TABLE 1. Description of various 2 × CO_2 experiments* referred to in the text.

Model	Duration	Warming	Comments	Name
GCMAM	50 yr	5.1°C	Calculated SSTs	S-C
GCMAM	10 yr	4.2°C	Specified SSTs (from T-S)	S-S
GCMAM	50 yr	5.1°C	S-C with O_3 feedback	S-O
GCMAM	5 yr following 10 yr spinup after S-O	5.1°C	S-O with PSC feedback on O_3	S-OP
GCM	35 yr	4.2°C	Standard run, calculated SSTs	T-S
GCM	30 yr	4.8°C	Alternate run with different sea ice formulation	T-A
GCMAM in trop. GCM in strat.	5 yr	4.9°C	SSTs from S-C	H
GCMAM minus mesosphere	5 yr	5.0°C	SSTs from S-C	-M

* All experiments have control runs of equal duration.

8° lat × 10° long horizontal resolution and 23 layers, extending from the surface to 85 km. It includes all the features of the GISS climate model (Hansen et al. 1983) and in addition has parameterizations for gravity wave drag due to topographic, convective, and shear forcing. The version used has calculated sea surface temperatures, with specified ocean heat transports (''q fluxes''), as described in Hansen et al. (1984) and Rind and Lonergan (1995). The primary model deficiencies are somewhat reduced planetary long-wave energy in the lower stratosphere, too cold temperatures near the model top, and too warm temperatures in the Southern Hemisphere polar lower stratosphere in winter (Rind et al. 1988a). Of these, the model's coarse resolution appears responsible for the reduced planetary wave energy; a new version of the model at 4° lat × 5° long resolution has significantly greater long-wave energy in the lower stratosphere. This deficiency may affect the conclusions concerning stratospheric warmings, as described below.

Comparison will be made with the standard GISS GCM experiments. The GCM has nine levels, a top at 10 mb, and a simplified drag in the top model layer (Hansen et al. 1983).

In the first experiment we instantaneously doubled the atmospheric CO_2 from 315 to 630 ppm and allowed the sea surface temperatures to adjust. To ensure equilibrium, both control and experiment were integrated for 50 model years. As indicated by both the global surface air temperature change, and the net radiative flux at the top of the atmosphere, the model reached equilibrium by about year 30; results shown will be the averages for the last 10 yr of each simulation.

In the second experiment, we again instantaneously doubled the atmospheric CO_2, but this time we incorporated a parameterization for stratospheric ozone response to changing atmospheric temperatures and overhead column ozone. The parameterization was calculated through the use of a 1D photochemical model applied at each latitude, with specified ozone transport convergences (paper 2). Note that this is not a complete ozone change experiment, which would include changes in ozone transports as well as changes in the photochemistry, composition, and transports of other species. It should therefore be looked upon as being a first-order feedback to the climate change induced by increased CO_2. However, an estimate of the effects of transport changes has been calculated offline and, as shown in paper 2, changes in the ozone transport convergences would not greatly alter the temperature change results. This experiment was also run for 50 yr with interactive sea surface temperatures.

In the third set of experiments, we included a parameterization for PSCs, in both a control run and the 2 × CO_2 run. The ozone changes that resulted are discussed in paper 2; here we concentrate on the climate impact of the change in ozone due to PSCs.

Finally, to assess the impact of vertical resolution and model top location, we make comparisons with previously published results from both the GCMAM and the GCM. Since these models differ in both respects, two hybrid models were generated. The first model had the vertical resolution of the GCMAM but the model top location of the GCM; this involved adding two levels to the GCM and rearranging the tropospheric resolution, in particular increasing the resolution in the boundary layer (three layers with mean pressure greater than 900 mb, as opposed to one layer in the GCM). The second model lowered the top of the GCMAM to 0.68 mb (about 50 km); hence the stratosphere was resolved but not the mesosphere. Both control and doubled CO_2 experiments were made with the new models, although the sea surface temperature changes due to increased CO_2 that were calculated with the full GCMAM were used for these doubled CO_2 simulations.

The different doubled CO_2 experiments are summarized in Table 1. Note that each experiment has a 1 × CO_2 control run as well, simulated for an equal number of years. The runs will be referred to by the name indicated in the right-hand column. The prefix ''S'' indicates runs using the model with the resolved stratosphere (and mesosphere) (GCMAM), while the prefix ''T'' indicates runs with the primarily tropospheric model (GCM). The hybrid resolution/top model is indicated with an ''H,'' and the GCMAM without the mesosphere is called ''-M.'' Sea surface temperatures were calculated in all experiments except S-S, H, and -M. The two

tropospheric experiments use different sea ice formulations and are discussed in detail by Hansen et al. (1984) and Rind et al. (1995). Results shown will be the last 10 yr of each experiment and control run, except for 5 yr in S-S, S-OP, H, and -M.

3. The doubled CO_2 troposphere–stratosphere with interactive sea surface temperatures

a. Calculated sea surface temperatures

The basic difference between the first experiment (S-C) and that described in paper 1 (S-S) is that now sea surface temperature changes are calculated directly. As described in paper 1, S-S was not in radiative equilibrium due to the prescribed sea surface temperature change; it was estimated that if the ocean temperatures had been allowed to adjust, the model warming would have increased from 4.2°C to about 5.1°C. It was further speculated that the additional warming was due to the greater vertical resolution in the GCMAM, which would allow additional upper-level cloud cover increase (a positive greenhouse effect).

In the new experiment (S-C) those predictions proved valid. In fact, the new run was 5.06°C warmer, on the global annual average, than the control run, with a 5% increase in upper-level cloud cover. Some of the differences shown below between S-C and S-S arise because of the greater warming in this simulation.

Figure 1 shows the zonal average temperature change for the annual average, December–February, and June–August mean, respectively, for the last 10 yr of the simulation. As expected, the troposphere warms and the stratosphere cools, although in the Northern Hemisphere (NH) some warming occurs in the extratropical stratosphere, especially in winter. Comparison with the results shown in paper 1's Fig. 1 for S-S indicates that the overall patterns are similar.

Figure 2 shows the difference in the temperature change by dynamics for the annual average and two solstice seasons [the diagnostic is calculated by assessing the temperatures before and after the dynamics subroutine]. The extratropical stratosphere and lower mesosphere are being warmed more dynamically, partially counteracting increased radiative cooling due to the additional CO_2. The tropical stratosphere is in general undergoing additional cooling. [Since these are equilibrium results, an overall balance is reached, so the changes induced dynamically are compensated for radiationally with the new equilibrium temperature shown in Fig. 1.]

The dynamical warming is associated with an increase in the residual (transformed Eulerian) circulation [Fig. 3, in which in the NH (Southern Hemisphere, SH) a negative (positive) value indicates a greater clockwise (counterclockwise) circulation in the frame of the figure]. In the lower middle stratosphere (~25 km) the percentage increase is quite large—on the order of 70%

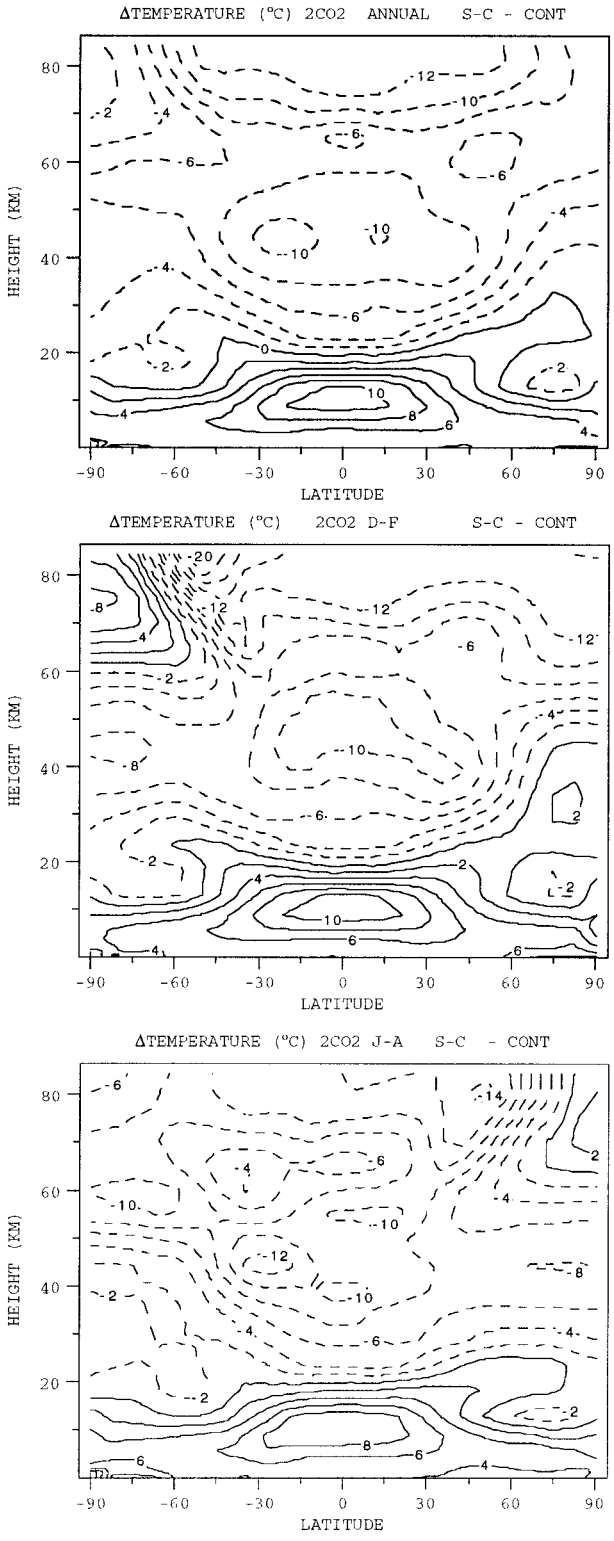

FIG. 1. Zonally averaged temperature change between the doubled CO_2 simulation (S-C) and the control run. Results are averages over the last 10 yr of 50-yr simulations. Shown are the annual average (top), December–February (middle), and June–August (bottom).

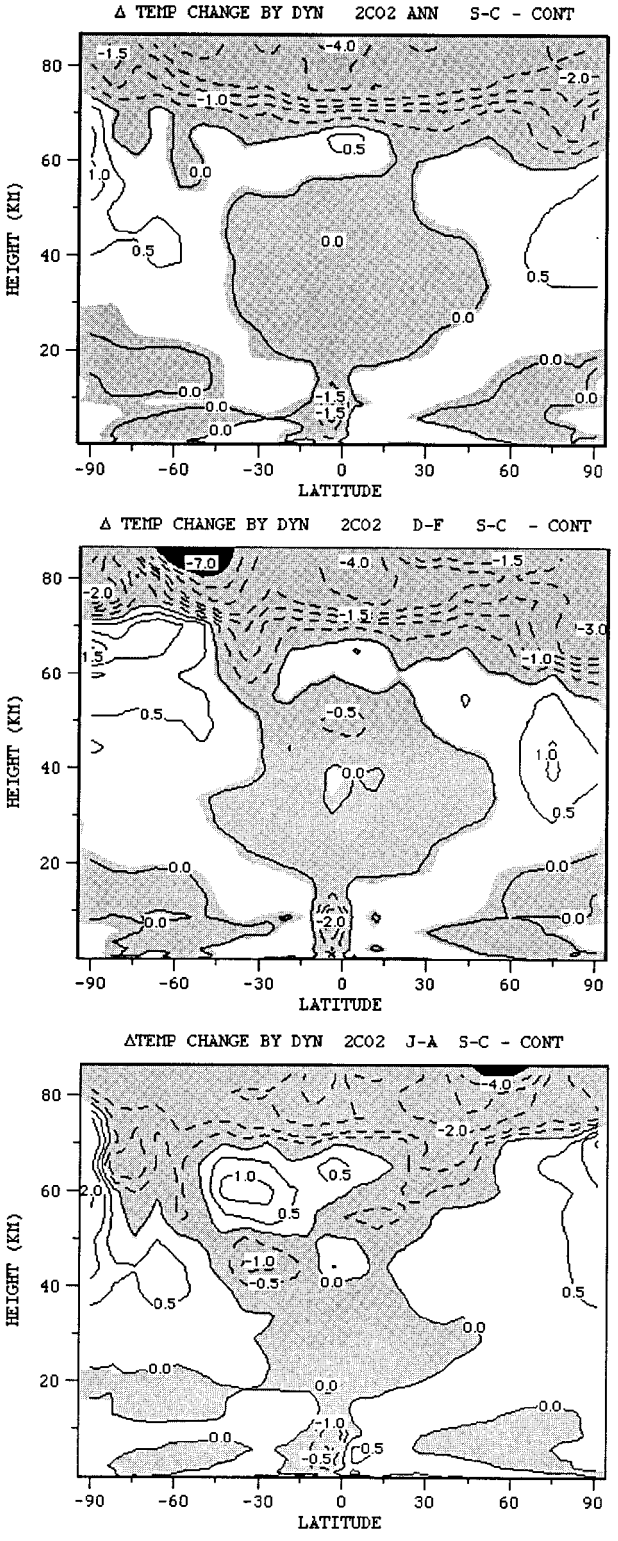

FIG. 2. As in Fig. 1 except for the change in dynamical effects on temperature. Regions less than zero are shaded (occasional mismatches result from interpolation).

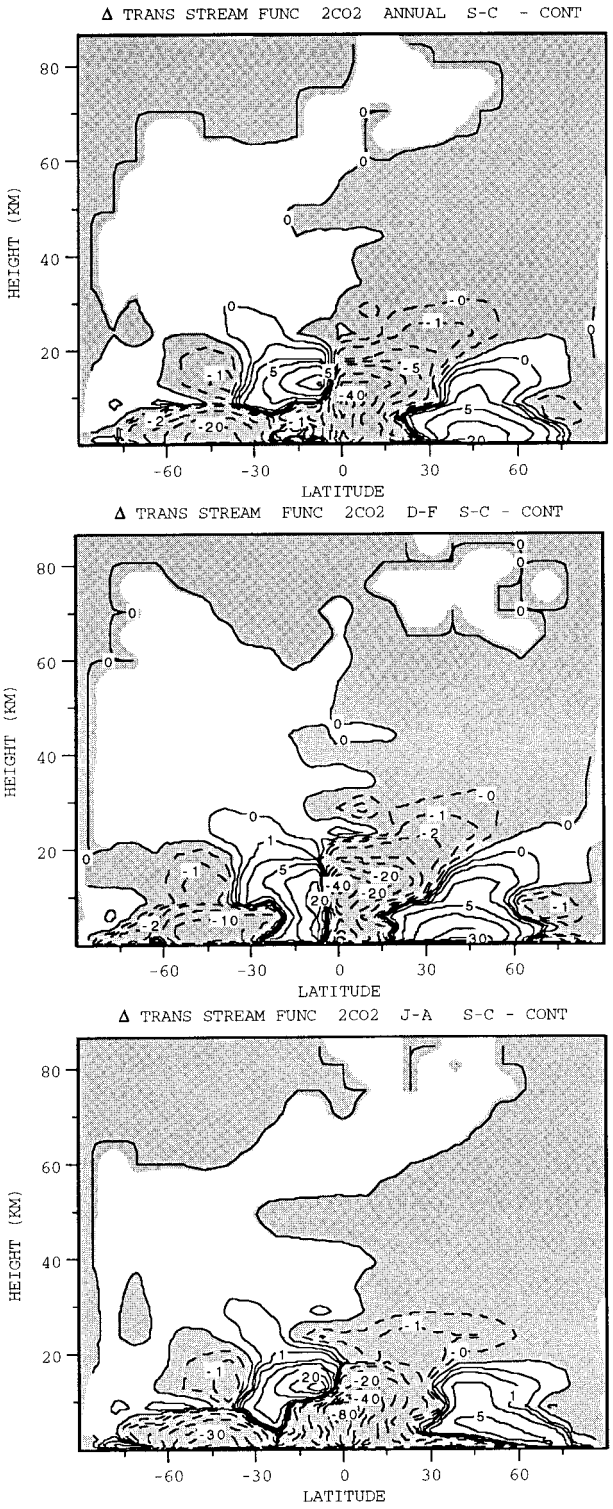

FIG. 3. As in Fig. 2 except for the change in the transformed Eulerian streamfunction (10^9 kg s^{-1}).

in the NH and 40%–50% in the SH for the annual average. Percentage changes are almost as large during the active winter seasons. These changes are larger than those that occurred in S-S, which annually averaged 10% of control run values. The percentage changes are much smaller in the lowest portion of the stratosphere and above the middle stratosphere.

The residual circulation increase is being driven by greater Eliassen–Palmer (EP) flux convergences in the upper stratosphere/lower mesosphere (Fig. 4) of up to 50×10^{-6} m s^{-2} (4 m s^{-1} day^{-1}) during December–February. These are often larger than the control run values and occasionally of opposite sign. The increased EP flux convergences are generating the stronger positive residual circulation in Fig. 3; the increased EP flux divergences in the lower stratosphere are associated with the increased negative circulation change that appears in the extratropical lower stratosphere in both hemispheres (note the opposite sign for positive circulation change in the two hemispheres).

The change in EP flux vectors producing this warming are given in Fig. 5. Evident is a relative equatorward flux in the low-to-midstratosphere, with an upward and poleward flux in the midstratosphere to lower mesosphere in both hemispheres. The explanation for this flux change can be derived from the zonal wind change (contours) also indicated in Fig. 5, which in turn relates to the temperature change shown in Fig. 1. Tropospheric warming in the model maximizes in the tropical upper troposphere, which results in an increased latitudinal temperature gradient in the altitude range from 500 to 100 mb. Hence the zonal winds at midlatitudes increase at these levels and above to the middle stratosphere. As the wind increase maximizes in the lower stratosphere, the change in the second derivative of the zonal wind with altitude, $\Delta\partial^2U/\partial z^2$, is positive, and $\Delta\partial q/\partial y$, the change of the quasigeostrophic potential vorticity gradient in the upper troposphere, is negative. From wave refraction theory, the more negative gradient is associated with an equatorward flux of wave energy in a region of west winds. Since the tropical warming is always greatest in the upper troposphere, the effect occurs in all seasons and both hemispheres. The effect dies away above the middle stratosphere, as $\Delta\partial^2U/\partial z^2$ becomes negative, $\Delta\partial q/\partial y$ becomes positive, and a greater poleward flux arises in the upper stratosphere. A similar result was shown for the Northern Hemisphere in paper 1.

As indicated in Fig. 1, the warming at low and midlatitudes is not restricted to the troposphere but extends to approximately 50 mb. It results from several different processes: advection of warmer air from the troposphere, greater subsidence in middle latitudes due to the increased residual circulation, and increased absorption of the greater radiative flux from the troposphere. It will have a negative effect on ozone tendencies, which vary in the opposite sense to the temperature change. In con-

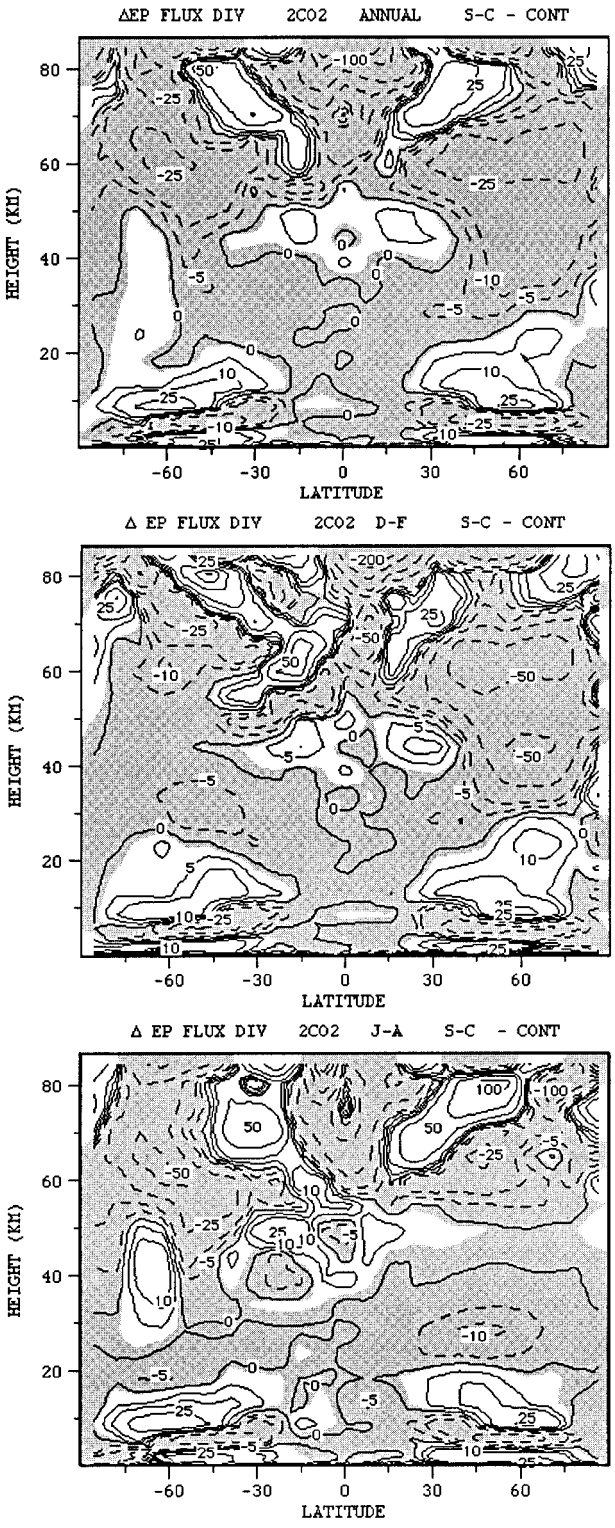

FIG. 4. As in Fig. 2 except for the change in the EP flux divergence (10^{-6} m s^{-2}).

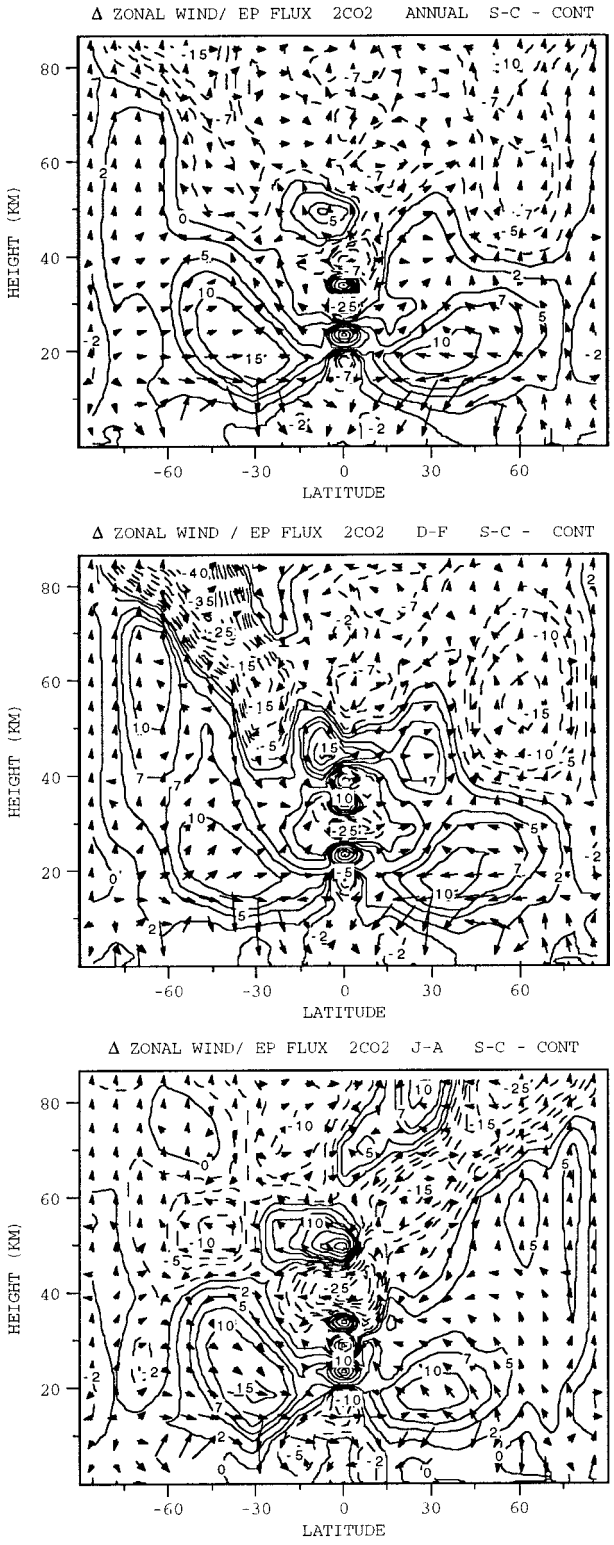

FIG. 5. As in Fig. 1 except for the change in the zonal wind (contours, m s^{-1}) and EP fluxes (arrows, 1 mm $\sim 10^{18}$ J).

trast, at higher latitudes cooling occurs down to 200 mb, which will impact PSC formation.

b. GCMAM versus GCM results

The emphasis so far has been on wave propagation changes as being responsible for the stratospheric circulation response; in paper 1 it was noted that increased generation of planetary long waves in the troposphere was also a contributing factor, which is contrary to expectations given the decrease in latitudinal temperature gradient with doubled CO_2. Does increased generation occur in this experiment as well? Shown in Table 2 are the global, annual average changes in eddy kinetic energy (EKE) for the longest planetary waves (waves 1–4) in the troposphere and for the total eddy energy in both the troposphere and stratosphere. Also given is the interannual standard deviation from the control run of T-S. Only the runs with increases in tropospheric long-wave energy have increases in lower stratospheric energy, and, while the changes are not necessarily proportional, the greatest increase (decrease) in stratospheric energy occurs with the greatest increase (decrease) in tropospheric long-wave energy. The propagation effect is illustrated in S-S, where the tropospheric long-wave increase is not significant, but the stratospheric EKE change is highly significant. Note that in H, tropospheric long-wave energy increases, but overall stratospheric energy decreases; we return to the results from H in the discussion section.

The results also highlight the difference between the GCMAM and GCM experiments. The increases in tropospheric planetary long-wave energy for both GCMAM experiments are significant relative to the two GCM decreased values, and the increases occur despite the strong decreases in total tropospheric eddy energy. We can diagnose this difference further by exploring the tropospheric energy budgets from the different experiments.

Shown in Table 3 are the contributing terms to the global, annual planetary long-wave eddy kinetic and eddy available potential energy (EAPE) budgets. Also shown are the zonal kinetic energy (ZKE) and zonal available potential energy (ZAPE) budgets. The transformation terms shown with arrows have the usual meaning. For the planetary long waves, it is not possible to determine whether energy lost through nonlinear interactions is going to the zonal-mean flow or to other wavenumbers, so the term is left ambiguous. ''Sinks'' for kinetic energy in the model include surface friction, mountain drag, and convective mixing of momentum. ''Sources'' for available potential energy include radiation, latent heat release, and surface fluxes. The interannual standard deviations are again shown in the right-hand column. [Note that the three contributing factors in each budget should add to zero; when they do not, it is because of sampling and round-off uncertainties.]

The GCMAM runs with increased long-wave eddy

TABLE 2. Change in annual global average eddy energy for wavenumbers 1–4 and total in 10^{17} J (%) in various doubled CO_2 experiments.

ΔEKE	S-C	S-S	T-S	T-A	H	Std dev
1000–100 mb (waves 1–4)	58.9 (3.9)	25.2 (1.6)	−93.2 (−1.9)	−122 (−7.9)	32.6 (2.2)	30.3 (2.0)
1000–100 mb (total)	−363 (−9.1)	−388 (−9.1)	−471 (−11.1)	−452 (−12.1)	−329 (−7.5)	41 (1.0)
100–10 mb (total)	72.8 (19.6)	40.6 (10.9)	−35.4 (−4.7)	−41 (−5.3)	−14.4 (−3.2)	7.7 (1.0)

kinetic energy all have increased generation from eddy available potential energy. In these runs, more EAPE is being generated due to interaction with other eddies and the zonal-mean flow.

Another difference is associated with the ZAPE itself, which increases in the GCMAM experiments and decreases in the GCM. The ZAPE increase is likely feeding EAPE through the nonlinear term. Therefore, the following scenario suggests itself: in the GCMAM, ZAPE acts as an increased source of energy for the longest waves, with energy transferred to EAPE (via the nonlinear terms) and then to EKE. In the GCM, ZAPE decreases, the nonlinear transfers in the longest waves are muted, and long-wave EKE generation and EKE itself are negative. The difference in long-wave eddy energy between S-C and T-A amounts to about 12% in the troposphere and close to double that for total lower-stratospheric eddy energy. Clearly the stratospheric response depends upon which version of the model is used.

The APE source terms are less negative in the GCMAM runs, especially in S-C. To understand this, we first indicate how the potential sources are affecting the total potential energy (TPE). The changes in the primary sources for TPE are given in Table 4. With warmer doubled CO_2 temperatures, there is increased condensation and latent heat release, a positive source for TPE in all the experiments. Radiation tends to damp the temperature changes and acts as a sink in all experiments. With warmer sea surface temperatures, latent heat is favored over sensible heat (the Bowen ratio decreases), so the surface interaction change is also a sink. In equilibrium, on the global average, there is near balance when one includes the much smaller terms (dynamics, sea level pressure filter). TPE increases in all the doubled CO_2 runs, approximately proportional to the magnitude of the warming in each run (Table 1). Generation of TPE by condensation is greatest in S-C, as are the radiational and surface losses.

ZAPE is generated when these source terms increase the temperature at low latitudes relative to high latitudes. The variation in the change of condensation latent heat release is shown in Fig. 6 (top). There is greater condensational heat release (and hence precipitation) increase in the Tropics in the GCMAM runs and a larger latitudinal gradient in its generation, especially in S-C. This is associated with a greater tropical latent heat flux from the surface (evaporation) (Fig. 6, middle), which helps fuel the condensational heat release. The increased tropical evaporation is due to the warmer tropical surface temperatures in S-C (Fig. 6, bottom); as noted earlier, the greater warming may arise from a greater increase in upper-level clouds possible with the increased vertical resolution in the upper troposphere.

These warmer tropical temperatures also explain the differences in the radiation and surface TPE and ZAPE sinks. With the warmer tropical sea surface temperatures, the sensible heat flux reduction is greatest in

TABLE 3. Change in tropospheric annual global average energetics for waves 1–4 and zonal-mean flow in various doubled CO_2 experiments (1000–100 mb). Energies in 10^{17} J, rates in 10^{12} W. Percentage changes in parentheses.

Energetics	S-C	S-S	T-S	T-A	H	Std dev
ΔEKE (Waves 1–4)	59 (3.9)	25 (1.6)	−93 (−6.3)	−122 (−7.9)	33 (2.2)	30.3 (2.0)
EAPE → EKE	30	13.5	−10	−6	34	13.3
Nonlinear	−31	−15	−17	−20	−37	15.1
Sinks	0.4	1.8	28	30	4	24.5
ΔZKE	848 (28.5)	442 (14.7)	103 (4.1)	156 (6.2)	742 (25.2)	35.9 (1.4)
ZAPE → ZKE	30	16	−11	−3	37	7.5
EKE → ZKE	5.5	9	15	13	−9	7.3
Sinks	−35	−25	−3.5	−10	−27	1.1
ΔEAPE (Waves 1–4)	−411 (−6.3)	−315 (−4.5)	−363 (−7.3)	−447 (−8.8)	−647 (−12.3)	22.7 (0.5)
EKE → EAPE	−30	−13.5	10	6	−34	13.3
Nonlinear	87	50	21.5	9	94	9.1
Sources	−59	−33	−28	−13	−60	8.0
ΔZAPE	993 (3.9)	312 (1.1)	−737 (−2.9)	−600 (−2.3)	278 (1.1)	246.8 (1.0)
ZKE → ZAPE	−30	−16	11	3	−37	7.5
EAPE → ZAPE	152	281	278	313	129	42
Sources	−118	−250	−286	−316	−113	38.6

TABLE 4. TPE changes in the doubled CO_2 simulations. Units 10^{-2} W m^{-2}. Percentage changes in parentheses.

TPE Budget	S-C	S-S	T-S	T-A	H	Std dev
TPE (10^5 J m^{-2})	519 (2)	408 (1.6)	394 (1.6)	447 (1.8)	570 (1.3)	12 (0.04)
Condensation	1477 (17)	1097 (13)	994 (11)	1096 (12)	1436 (17)	55 (0.5)
Radiation	−1077 (−9)	−739 (−6)	−671 (−6)	−762 (−7)	−970 (−8.5)	41 (0.4)
Surface	−386 (−12)	−303 (−9)	−329 (−13)	−326 (−13)	−464 (−15)	16 (0.6)

S-C (Fig. 7, top), with the difference maximizing in the Tropics (hence reducing ZAPE). The warmer tropical temperatures also produce greater longwave and total radiational cooling in the Tropics relative to high latitudes (Fig. 7, bottom), again a greater loss of ZAPE. However, the condensational source change is more important, and the net effect is a smaller negative source for ZAPE in the GCMAM (Table 3), a total gain in ZAPE, and the subsequent energy cycle effect on EKE.

What about the other experiments? In light of the above explanation, it is interesting to compare S-S and T-S, which both use the same sea surface temperatures. The ZAPE increase in S-S is not significant, yet it is significantly more positive than the GCM changes (Table 3). Furthermore, there are still increases in tropospheric longwave EKE and its generation in S-S, again significant relative to the GCM results. Experiment S-S does have some increase in tropical condensation relative to high latitudes (Fig. 6, top), and somewhat less tropical radiative cooling loss (Fig. 7, bottom). In addition to having a fully resolved stratosphere, the GCMAM also has increased vertical resolution in the troposphere compared with the GCM, both in the boundary layer and in the upper troposphere. The finer-resolution magnifies moist convective mass fluxes, as stability is reduced with thinner atmospheric layers; see, for example, how radon with a source at the surface increases in the upper troposphere in GISS GCM experiments with greater vertical resolution (Rind and Lerner 1996). Similarly, in the climate change experiment, the finer vertical resolution also gives rise to enhanced instability, with the global rainfall increase about 10% larger in S-S than T-S, hence the amplification of the condensation contribution to ZAPE in S-S. Increased tropical high clouds occur in S-S due to the increased vertical resolution, limiting the tropical longwave cooling sink of ZAPE. The net effect is to produce a more positive ΔZAPE in S-S. Note that these resolution effects are obviously playing a role in S-C as well.

Experiment T-A has greater warming than S-S or T-S, almost as much as S-C, but the tropical warming is not as amplified (Fig. 6, bottom). The additional warming originated from a change in the sea ice melting parameterization (Rind et al. 1995) so it is in the SH sea ice area that the temperature effect is maximized. Thus it is not simply the magnitude of the $2 \times CO_2$ warming response but its latitudinal gradient that is important (and vertical gradient as well, which affects stability and condensation, in addition to APE directly). Since the tropospheric tropical warming is also important for changing the lower-stratospheric refractive properties, it is involved in both mechanisms affecting stratospheric eddy energy and the residual circulation. We return to this point in the discussion section.

What difference does the increase in tropospheric longwave energy in the GCMAM simulations compared to those of the GCMs have on the tropospheric simulation of the doubled CO_2 climate? Planetary long waves have the potential to transport energy poleward; for example, Kao and Sagendorf (1970) calculated that during the winter of 1964, the poleward sensible heat transport was accomplished primarily by waves 1–4. Therefore, the different tropospheric long-wave responses in the GCMAM and GCM might result in different energy transports, affecting the climate change itself.

To examine this possibility, shown in Fig. 8 (top) is the annual average change in moist static energy transport (the sum of sensible heat, latent heat, and geopotential energy) by eddies. The GCMAM has larger poleward eddy transports in the extratropics, consistent with its greater eddy energy; while some of the differences are associated with the different magnitudes of warming, S-S and T-S have similar temperature increases, and T-A has more warming than S-S. The change in moist static energy transport by the atmosphere (eddies plus the mean circulation) is given in Fig. 8 (bottom). Additional changes are apparent in low-latitude transports. The change in condensational heat release shown in Fig. 6 (top) results in differing responses of the Hadley circulation in the different experiments, which then affects mean circulation transports as well. These results emphasize that the actual climate response is influenced by the differing dynamical changes in these experiments.

c. Sudden stratospheric warmings

Stratospheric warmings have long been known to be associated with significant ozone changes (e.g., London 1963; Zullig 1973; Degorska and Rajewska-Wiech 1996). Austin et al. (1992) concluded from their modeling results that if only a late stratospheric warming occurs in the doubled CO_2 atmosphere, then an intensified Arctic ozone hole is likely. In paper 1 it was noted that there appeared to be an alteration in the timing of sudden stratospheric warmings, which occurred earlier and then again later in the doubled CO_2 experiments. It was speculated that this might have resulted from either the increased eddy energy in the stratosphere (the preferred explanation) or the additional radiative destabilization associated with increased CO_2. However, the

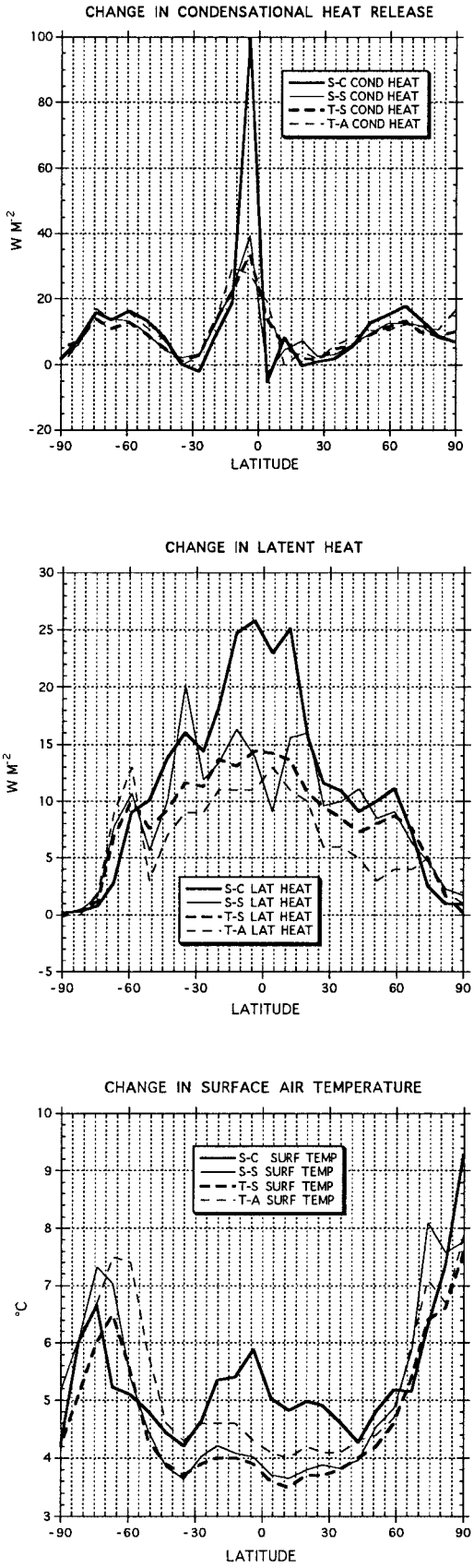

FIG. 6. Change in annual average condensational heat release (top), latent heat flux from the surface (middle), and surface air temperature (bottom) with the different GCM and GCMAM experiments.

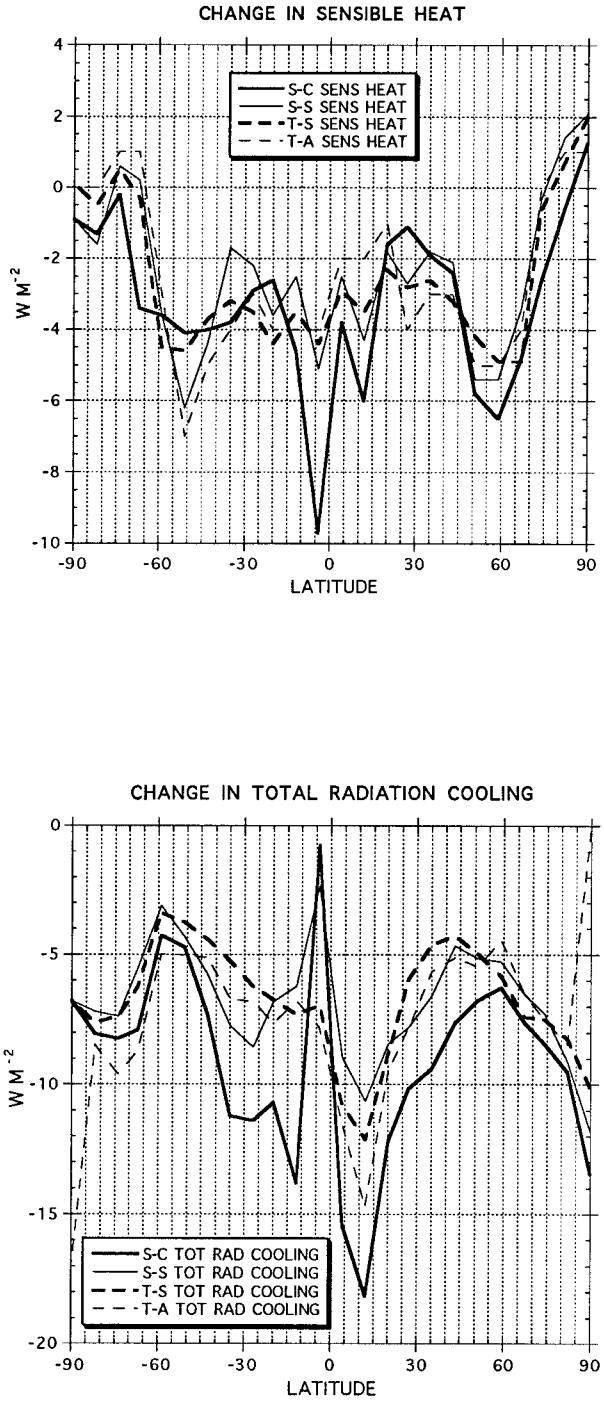

FIG. 7. As in Fig. 6 except for sensible heat flux from the surface (top) and total radiation cooling (bottom).

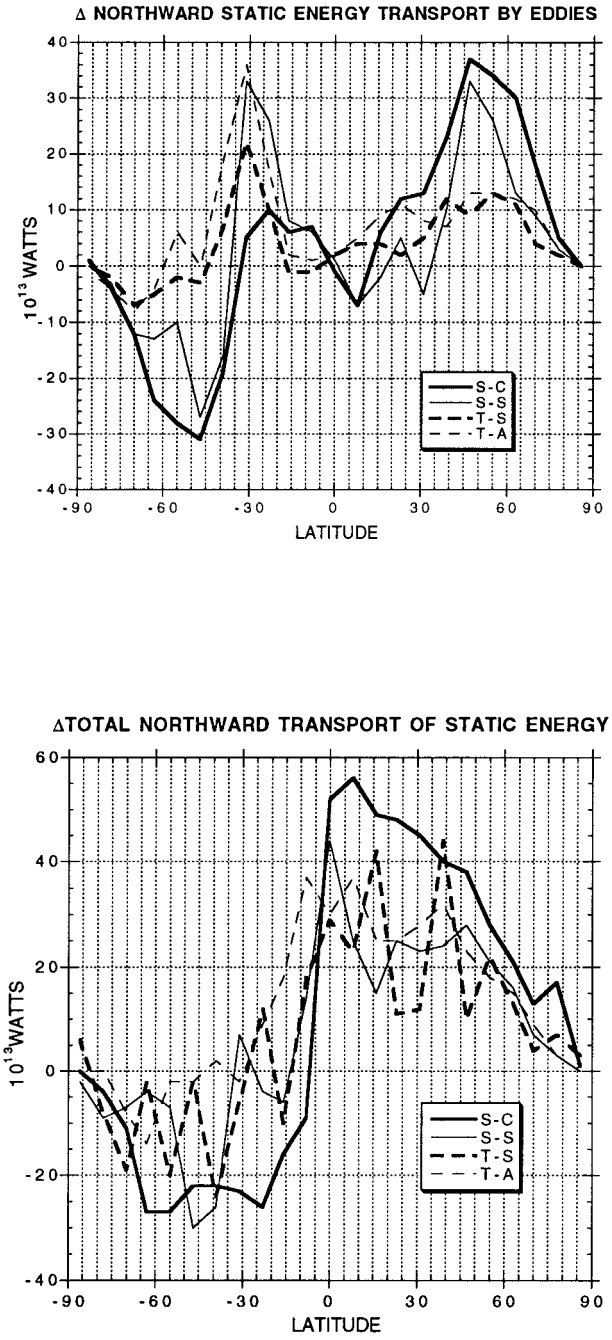

FIG. 8. Change in northward transport of static energy by eddies (10^{13} W) (top) and by the atmosphere (mean circulation plus eddies, 10^{14} W) (bottom) in the different GCM and GCMAM experiments.

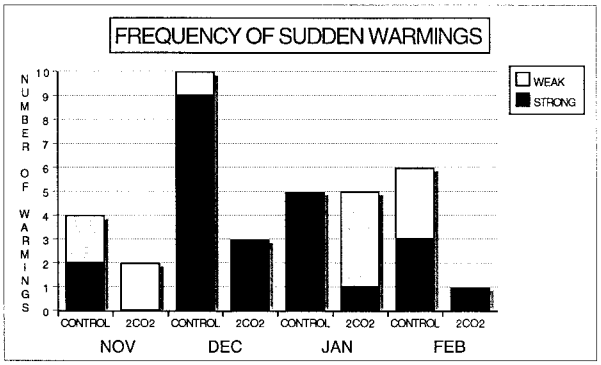

FIG. 9. Frequency of sudden stratospheric warmings in the control run and doubled CO_2 simulation (S-C). Both strong and weak events, as defined in the text, are shown.

sample was too small to draw meaningful conclusions. In these experiments we have 50 yr for both the control and the experiment, which allows for a more significant appraisal of changes in stratospheric warmings. We restrict the discussion to the last 25 yr of S-C and its control, when the doubled CO_2 simulation was in approximate equilibrium; only NH events are reviewed, as the model does not simulate warmings of this nature in the SH, nor do they generally occur in the real world.

The GCMAM develops stratospheric warmings that generally occur above the 10-mb level (Rind et al. 1988b), perhaps due to the underestimation of planetary long-wave energy in the lower stratosphere with the model's coarse resolution. Balachandran et al. (1998, submitted to *J. Atmos. Sci.*) show examples of the occasional model warmings that do propagate down to below the 10-mb level, however, and would then qualify as ''major warmings.'' Comparison of the model's temperature and wind changes with time, the more usual criteria for discerning stratospheric warmings with hemispheric energy diagnostics, suggest the following conditions for GCMAM warmings: in the region between 10 and 1 mb, hemispheric zonal kinetic energy must be reduced by more than a factor of 2 within a 10-day period, and hemispheric eddy kinetic energy must grow to exceed 10^{19} J.

In the control run, these requirements are met 19 times during the last 25 yr of the simulation; in addition, another six times the requirement is almost met (''weak events''). In the doubled CO_2 simulation, warmings occur only five times during the last 25 yr, with an additional six weak events. Hence warmings decrease in the doubled CO_2 climate; the timing of the events shows little systematic change (Fig. 9). In addition, in the control run, 10 of the events had hemispheric eddy kinetic energy in the 10–1-mb region exceeding 125×10^{17} J; that happened just once in the $2 \times CO_2$ simulation.

In the GCMAM control run, 11 of the 20 strong warmings are primarily wave 2 events, and five others are combined wave 1 and wave 2. The model appears to react more suddenly to wave 2 energy triggering; this may be a result of the model's coarse resolution. In the doubled CO_2 climate, all five strong warmings are wave 1 events (hence there are more wave 1 events than in the control), whereas the six weak events are all wave 2. The increase in lower-stratospheric eddy energy shown in Table 2 extends up to the 10–1-mb region as well, but not for wave 2. During NH winter, standing

wave 2 energy from 40° to 70°N increases by 15% at 30 mb, but it decreases by 8% at 10 mb and by 26% at 3.4 mb. Overall, wave 2 energy in the NH winter increased by 32% in the region from 100 to 10 mb, but decreases by 16% in the 10–1-mb region. The zonal wind increases that occur in the middle stratosphere (Fig. 5) appear to be prohibiting wave 2 energy from propagating above the middle stratosphere. Wave 1 is somewhat more immune to the zonal wind increase, as would be expected due to its better propagation characteristics through regions of west winds. For the winter seasonal average, standing wave 1 energy in the region 40°–70°N increases by 24% at 30 mb, 48% at 10 mb, and by 26% at 3.4 mb. Overall, wave 1 energy increases by 55% from 100 to 10 mb, and by 16% from 10–1 mb. (Effects similar to those reported here for both waves 1 and 2 in S-C occur in S-S.) Since the strong GCMAM events are preferentially wave 2 phenomena and occur in the region above 10 mb, the effects are selected against in the 2 × CO_2 simulation.

Notice that despite reduced sudden warmings, on the seasonal average there is greater EP flux convergence, and dynamically induced warming in the winter polar region (Figs. 2 and 4) associated with the large wave 1 increase. One hypothesis would be that sudden warmings would be modified if the strength of the polar vortex is substantially changed. Examination of the seasonal averages shows that in fall, the polar vortex is stronger by about 10%, whereas in winter it is basically unchanged.

4. Doubled CO_2 with ozone feedback

The mid- and upper-stratospheric cooling seen in Fig. 1 should lead to ozone increases, as ozone photochemical formation is favored when temperatures are lower. Ozone changes also depend upon the availability of UV radiation; when ozone increases aloft, less radiation penetrates to lower levels, with less ozone generation. In addition, at lower stratospheric levels throughout low and middle latitudes temperatures increase, which tends to decrease ozone. The annual average ozone change that results is given in Fig. 10 and discussed more fully in paper 2.

Figure 11 (top) shows the annual average temperature change compared to the control run in this combined CO_2–ozone change experiment (S-O). Figure 11 (bottom) shows the difference between this experiment and S-C. The ozone increase in the upper stratosphere results in a warming of several degrees; hence the upper-stratospheric cooling has been reduced by about 20%. The ozone decrease in the tropical lower stratosphere results in a temperature decrease of about 0.5°C, reducing the magnitude of warming there.

Ozone increase at high altitudes would tend to cool the climate, since less solar radiation will pass through the tropopause (Lacis et al. 1990). The change in solar heating rates between S-O and S-C is given in Fig. 12; the effect on the troposphere is minimal. The ozone decrease in the lower stratosphere is also a cooling effect, as it reduces the greenhouse capacity of the atmosphere (Lacis et al. 1990). Shown in Table 5 are the relevant radiation parameters, and climate response, as the difference between S-O and S-C. The total effects on both shortwave and longwave radiation are quite small, in fact they are less than the model's interannual standard deviations at the surface. Stratospheric ozone changes in general appear to be less effective in influencing surface temperature than would be expected by the radiative forcing at the tropopause, due to the changes it induces in upper-level clouds (Rind and Lonergan 1995; Hansen et al. 1997).

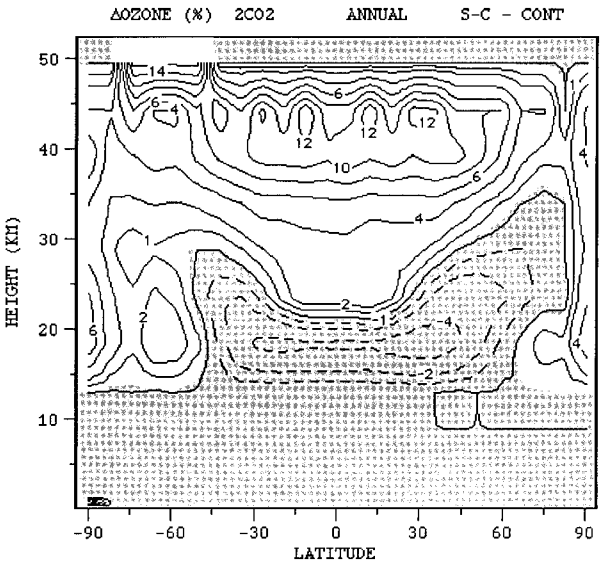

FIG. 10. Annual average changes in ozone (%) due to doubling atmospheric CO_2.

Surface air temperatures, relative to S-C, warm by 0.03°C, which is within the model's natural variability—this is therefore the effect of the ozone changes shown in Fig. 10. Cooling of up to a few tenths of a degree Celsius occurs in the Tropics, where the lower-stratospheric ozone decrease and upper-stratospheric ozone increase have maximum effect. The extratropics in general warm by up to a few tenths of a degree Celsius. The relatively small temperature changes that arise have little influence on the dynamical changes discussed above.

As noted in section 2, the ozone calculation does not include transport changes. An offline assessment of the transport effect is discussed in paper 2. When these calculated ozone changes were input to the GCM, the effect on the temperature and dynamics was minimally different from the results shown here. Nevertheless, had the dynamical ozone (and other species) transport changes been included online, the effect might have been somewhat different.

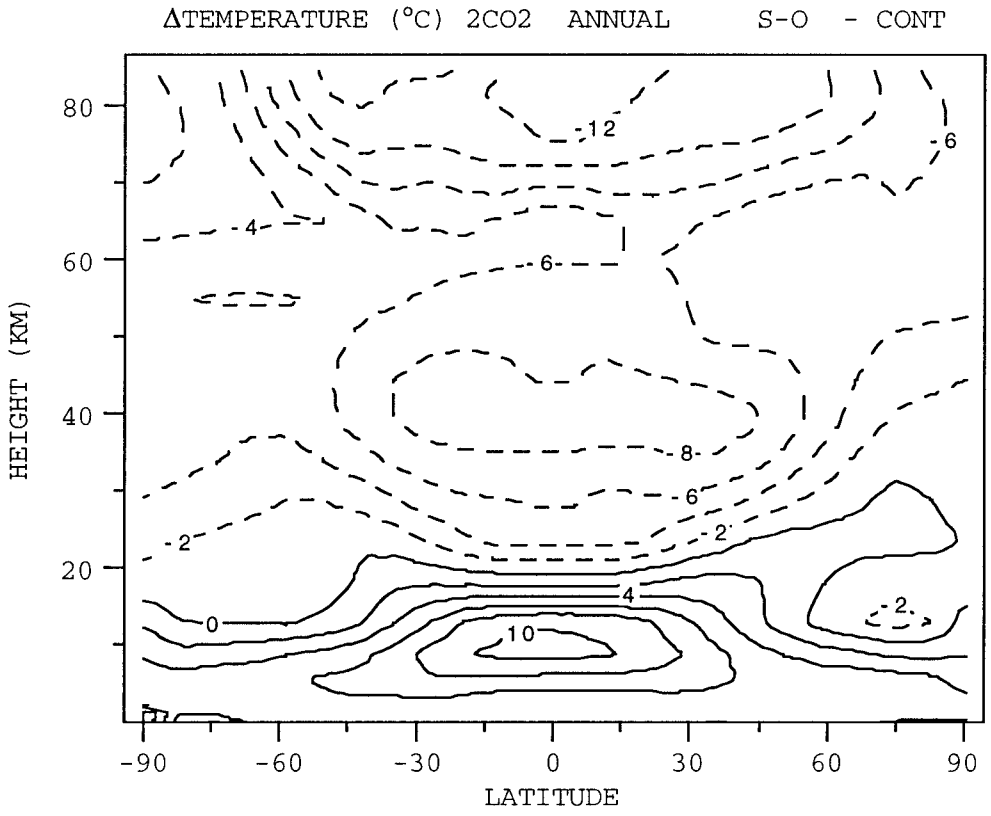
ΔTEMPERATURE (°C) 2CO2 ANNUAL S-O - CONT
HEIGHT (KM)
80
60
40
20
-12
-6
-4
-6
-8
-6
-2
-2
4
-2
0
10
-90
-60
-30
0
30
60
90
LATITUDE

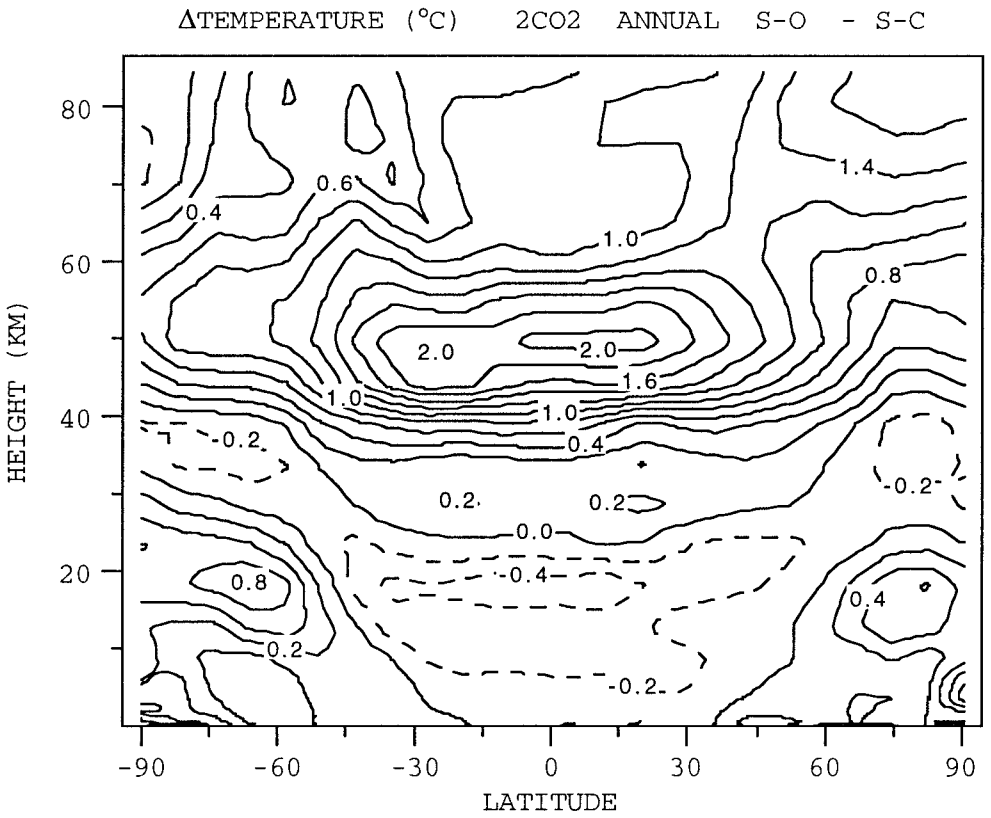
ΔTEMPERATURE (°C) 2CO2 ANNUAL S-O - S-C
HEIGHT (KM)
80
60
40
20
1.4
0.6
0.4
1.0
0.8
2.0
2.0
1.6
1.0
1.0
0.4
-0.2
-0.2
0.2
0.2
0.0
0.8
-0.4
0.4
0.2
-0.2
-90
-60
-30
0
30
60
90
LATITUDE

5. Doubled CO_2 ozone experiments with PSC formation

As discussed in paper 2, a PSC parameterization was included in both a control run and doubled CO_2 experiment. Briefly, both the control and doubled CO_2 simulation with ozone feedback (S-O) were extended for 10 yr with the GCMAM but reducing the parameterized mountain wave drag to one-fourth of its effect. As noted in Rind et al. (1988a), inclusion of the mountain wave drag results in too warm conditions in the south polar lower stratosphere during winter–spring. Reducing the wave drag allows the temperatures to return to observed values in the control run, although the simulation is degraded in other seasons and at other latitudes. For the sake of an experiment whose prime aim is to investigate PSCs, it produces a much more realistic climatology. The control and doubled CO_2 were then extended for an additional 5 yr allowing PSCs to form whenever the local temperature in the lower stratosphere dropped below 195 K; the PSC formation then led to ozone reductions. The PSCs were not allowed to have any direct radiative influence (which is expected to be quite small, since their optical thickness is on the order of 0.01), and therefore the effect on the doubled CO_2 climate sensitivity results not from the increase in PSCs that occurred, but through the PSC influence on ozone and its radiative response.

Inclusion of PSCs along with doubled CO_2 cooling in the polar lower stratosphere resulted in greater ozone loss in those regions when current stratospheric chlorine levels are maintained (Fig. 13). The absolute temperature change, and the temperature change relative to S-O is given in Fig. 14. Larger temperature reductions occur in the regions and seasons with greater ozone loss; maximum effect occurs in the polar lower stratosphere during spring in each hemisphere, where cooling of some 13°C occurs.

The cooling results from two processes. The loss of ozone itself generates cooling, due to the reduction in greenhouse capacity for longwave radiation. In addition, there are also dynamical changes induced by the ozone hole that amplify and spread the effect to other latitudes and altitudes. With a greater latitudinal temperature gradient, stronger west winds result, altering the atmospheric refraction pattern for planetary waves, affecting the residual circulation and hence dynamical warming. The positive temperature change by dynamics in the polar winter now occurs only in the upper stratosphere and lower mesosphere, where its effect is greater; planetary long-wave energy now increases more strongly at these levels and less strongly in the lower stratosphere (the lower stratospheric eddy energy increase is only one-half as large in S-OP as it is in S-O). This same effect also results in relative warming in the subtropical stratosphere (Fig. 14, bottom); with less dynamical warming in the polar lower stratosphere, there is less dynamical cooling at lower latitudes. The streamfunction change shown in Fig. 3 still occurs, although it is not as strong.

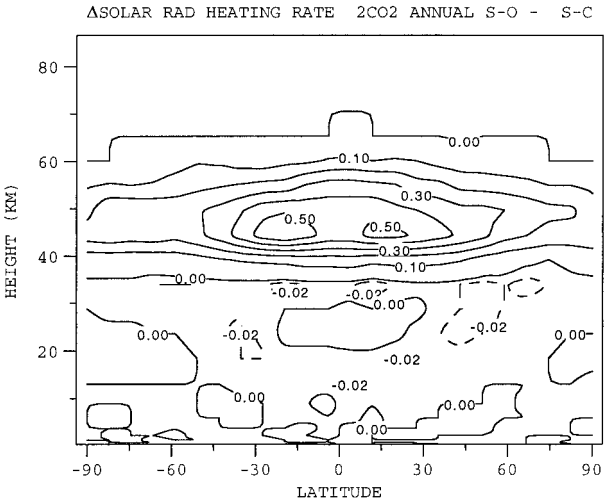

FIG. 12. Change in solar radiation heating rates (°C day^{-1}) due to the ozone changes shown in Fig. 10.

In the troposphere, the differences are small and primarily in the polar regions. Radiatively there is some compensation: when the ozone hole difference is a maximum, it is because sunlight has returned to the region, and with reduced ozone absorption, more sunlight gets into the troposphere; however, the reduction in ozone also allows more longwave radiation to leave the troposphere. Overall, there is a small relative warming in the polar troposphere in both hemispheres compared with S-O, although there is little effect on global mean temperatures.

6. Discussion

The primary results from paper 1 have been reproduced in these new experiments: in the doubled CO_2 climate, stratospheric eddy energy increases, as does the residual circulation, and tropospheric planetary longwave energy increases as well. The stratospheric changes appear to be the result of both altered propagation, due to warming in the tropical upper stratosphere, and altered generation of planetary long waves in the troposphere, also affected by the tropical warming. Lower-stratospheric warming occurs in the Tropics, with cooling at high latitudes, the latter effect leading

←

FIG. 11. Annual zonal-averaged change in temperature due to doubled CO_2 with ozone response (top); difference between the doubled CO_2 temperature change with and without ozone response (bottom).

TABLE 5. Tropospheric changes between S-O and S-C doubled CO_2 results.

Parameter	Units	Δ (S-O − S-C)	Std dev
Shortwave absorbed at 1.5 mb	W m^{-2}	0.05	0.01
Shortwave absorbed at surface	W m^{-2}	−0.08	0.24
Net radiation at surface	W m^{-2}	−0.1	0.3
Net heating at surface	W m^{-2}	−0.3	0.36
Surface temperature	°C	0.03	0.09

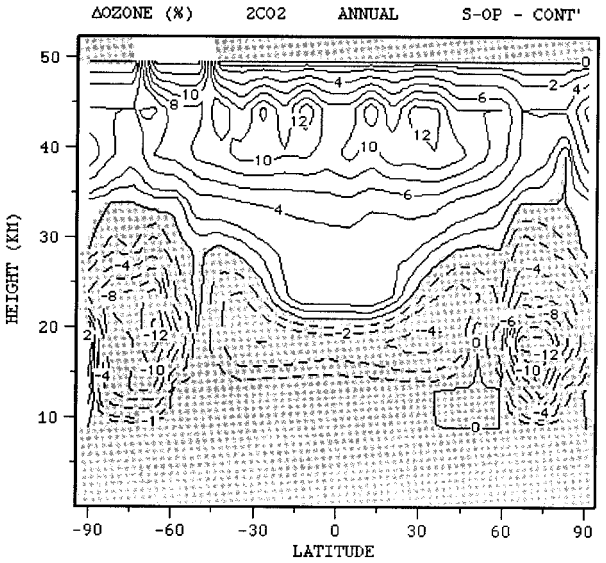

FIG. 13. As in Fig. 10 except for ozone changes with polar stratospheric clouds included.

to a greater frequency of polar stratospheric clouds. Stratospheric warmings decrease in frequency due to a reduction in wave 2 energy above 30 mb. Allowing for a crude ozone feedback reduces the upper-stratospheric cooling by about 20% but otherwise does not affect these conclusions; inclusion of the PSC response decreases ozone somewhat further in the polar lower stratosphere and reduces the doubled CO_2 dynamical warming there. In this section we discuss whether these results are likely to be found in other GCMs, and speculate as to whether they are likely to occur in the real world.

The comparison of the different GCM and GCMAM doubled CO_2 simulations, both in these experiments and those from paper 1, indicate what model characteristics are necessary to produce the stratospheric eddy energy and residual circulation increases. Both the generation and propagation effects seem to be associated with the magnitude of the tropical warming. The GISS model produces a substantial tropical response, both at the surface and in the upper troposphere. It was noted in paper 1 that in a GCMAM experiment with a different distribution of warming (i.e., much less in the Tropics, more at high latitudes), tropospheric ZAPE decreased strongly, and the effect on tropospheric and stratospheric long-wave energy was smaller or nonexistent. Therefore, models with reduced tropical warming relative to that at high latitudes are not as likely to produce the stratospheric circulation changes, although, as indicated in paper 1, the stratospheric cooling by itself (with no tropospheric response) did produce a tropospheric wave 1 response, and a smaller increase in stratospheric EKE. The key appears to be the magnitude of warming in the tropical upper troposphere, which is generally related to the warming at the surface; however, Boer (1997), using the Canadian Centre for Climate Modeling (CCC) GCM, found that substantial tropical upper-tropospheric warming resulted in increased ZAPE in the upper troposphere, and greater standing wave energy in the lower stratosphere, despite an overall reduction in tropospheric ZAPE due to minimal tropical surface warming.

Since it is not certain what the real world's latitudinal climate sensitivity is, or its vertical distribution, it would be hard to predict the reality of these effects. In a doubled CO_2 experiment (with, however, only a 1.4°C warming in the troposphere, derived from a transient atmosphere–ocean model simulation), Mahfouf et al. (1994) simulated a number of the features shown here, including dynamical warming of the polar stratosphere and an increased stratospheric Eulerian circulation.

The GCMAM differed from the GCM in two ways: greater resolution in the troposphere and greater resolution of the stratosphere with a raised model top. Some of the differences between those models might be attributable to each configuration. How the results vary with the vertical resolution in the troposphere, and whether the stratosphere has to be resolved to the extent it is in the GCMAM (top at 85 km) are important questions for model formulation. To differentiate the two influences, we first examine the results from H, using the sea surface temperature changes from S-C, with the vertical resolution in the troposphere of the GCMAM but as poorly a resolved stratosphere as in the GCM (top at 10 mb).

As shown in Tables 3 and 4 for H, the basic tropospheric dynamical processes described above are fairly similar to what occurred in S-C, and the GCMAM in general: increased ZAPE, nonlinear transfer to EAPE, and conversion to EKE. Hence they are a product of the tropospheric vertical resolution, and in particular, a better resolution of the boundary layer and upper troposphere; as noted earlier, the magnified moist convective flux associated with finer vertical resolution is a key to this result. Using the sea surface temperature changes from S-C, the increased TPE from condensational heat release in H is very similar to that in S-C (Table 4), as are the changes in latent and sensible heat flux and surface air temperature (values are close to those shown in Fig. 6 for S-C). The tropospheric EKE change in wavenumbers 1–4 is not quite as large as in S-C, but it is still much different from the GCM runs

with the same model top. Large increases also occur in eddy and total energy transport.

Here H was not in precise radiation balance and would have cooled by 0.5°C or slightly more had the sea surface temperatures been allowed to adjust; hence it would have been up to 15% cooler than S-C. The reason for this change is that cloud cover especially between 500 and 200 mb decreased slightly more in this experiment than in S-C, which allowed for more outgoing longwave radiation loss (while not having a significant impact on planetary albedo). The moisture in these levels did not increase as much in H; the reason appears to be that the moist convective mass flux went to higher levels in H, and the region between 500 and 200 mb experienced greater subsidence and drying. This difference existed in the control runs for H and and S-C as well; the upper troposphere–lower stratosphere is 17% less stable in H with the top of the model at 10 mb. The ability of the location of the top of the model to influence upper-troposphere convective fluxes is also occurring in ongoing experiments using radon as a tracer. Hence overall climate sensitivity, as influenced by upper-level convection and clouds, is affected by the location of the model top even with similar vertical resolution.

What does *not* occur in H is the increase in lower stratospheric eddy energy overall (Table 2) [although there is a small (5%) increase in the energy of wavenumbers 1–4]. Overall, the stratospheric results are somewhat in between that of the GCMAM and the GCM. Therefore, even with increased tropospheric eddy energy, placement of the model top in the middle stratosphere apparently inhibits the propagation of this energy into the stratosphere. As shown below, also missing is the large increase in stratospheric residual circulation. Therefore, proper resolution in the stratosphere, and location of the top of the model above the middle stratosphere, are requirements for producing a consistent stratospheric response.

This experiment does not resolve exactly how high the model top has to be. To address that question, we can explore the results in -M, which with a top at 50 km is in-between the ~30-km top of the GCMAM and ~85-km top of the GCMAM. Shown in Table 6 is the change in residual circulation at representative latitudes in the lower stratosphere. With a top at 10 mb (as in H), both the effects at 100 and 46 mb are diminished relative to S-C (whose sea surface temperatures it uses). It is conceivable that increased vertical resolution between 100 and 10 mb might allow some of the effects to be maintained, especially in the lowest stratosphere. In contrast, the results in -M are very similar to those in S-C, and this is true for the eddy energy increase associated with the longest planetary waves as well. Hence resolving the mesosphere is not necessary to produce the low-to-midstratospheric response to doubled CO_2; therefore many of the AMIP models might be appropriate for such simulations. Only in the upper stratosphere, near the model top, does the response in -M depart from that in S-C, and even there it generally captures qualitatively the circulation change. Similarly, with the model top at 50 km, the upper troposphere convection and cloud cover changes in -M are similar to those in S-C, and model sensitivity is more similar.

Boer (1997) discussed the concept of ''eddy efficiency,'' relating the change in total atmospheric energy transport to the change in eddy energy. In doubled CO_2 experiments with the CCC, he noted that eddy efficiency increased because of greater latent heat transport in the warmer climate. The same result occurs in these experiments as well, but it is dependent on the magnitude of the tropical warming and the vertical resolution. Tropospheric eddy energy decreased in all the experiments (Table 2), yet eddy static energy transport increased (Fig. 8, top). The increase was greater in S-C than in S-S, as S-C had larger tropical and overall warming. The increase was also larger in S-S than in T-S, despite their similar magnitude of tropical warming, because of the greater vertical resolution in S-S, and hence the greater latent heat release and planetary long-wave energy in that run. The model top location plays little role, as H and S-C had similar magnitudes of increased eddy efficiency.

Stratospheric cooling due to increased CO_2 is a fairly certain phenomenon, and therefore the cooling in the polar regions, with the concomitant PSC increases, is also reasonable. However, the magnitude of the response is open to question. This experiment was conducted with current chlorine levels. Since stratospheric chlorine levels are expected to peak in the first few decades of the twenty-first century and decline subsequently, while doubled CO_2 equilibrium forcing and response should not occur until close to year 2100, this experiment overstates the magnitude of the likely effect. In addition, as discussed in paper 2, and in the simulations of Austin and Butchart (1994), increases in the Arctic ozone hole depend upon the modeled reduction in stratospheric warmings, which lead to an undisturbed polar vortex.

In the real world, stratospheric warmings are more associated with wave 1 than wave 2, although there is significant interaction between the two during the course of an event. Therefore, the GCMAM result of decreased warmings, associated with decreased wave 2 energy, may overstate the effect, although a reduction in wave 2 energy would likely play some role (O'Neill and Pope 1988). Whether the large increase the GCMAM finds for wave 1 would compensate is open to question; Mahfouf et al. (1994) found that the increased wave activity led to an increase in stratospheric warmings in their simulation.

The ozone response to the CO_2-induced temperature changes appears reasonable compared to other model results, as shown in paper 2, despite the simplifying assumptions made in the approach. The climate response to these ozone changes also appears reasonable; the in situ temperature changes due to increased ozone are consistent with those found in other models, as dis-

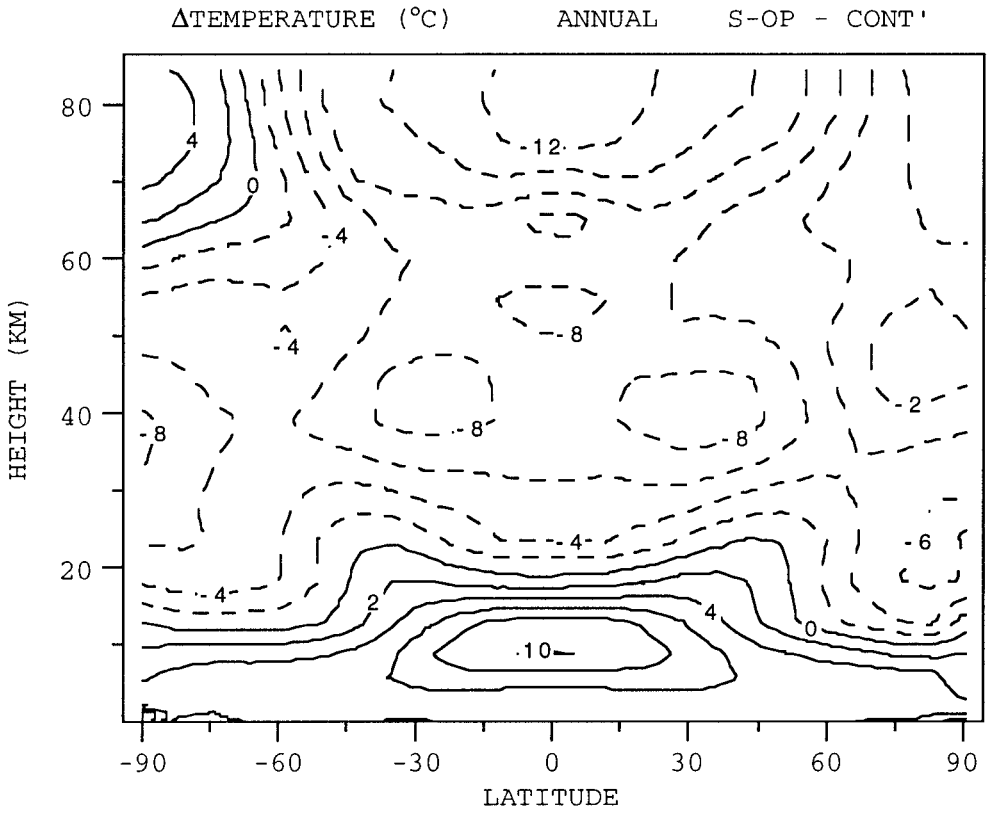
ΔTEMPERATURE (°C) ANNUAL S-OP - CONT'
HEIGHT (KM)
80
60
40
20
-90
-60
-30
0
30
60
90
LATITUDE
4
0
-4
-12
-4
-8
-8
-8
-2
-8
-4
-6
-4
2
4
0
10

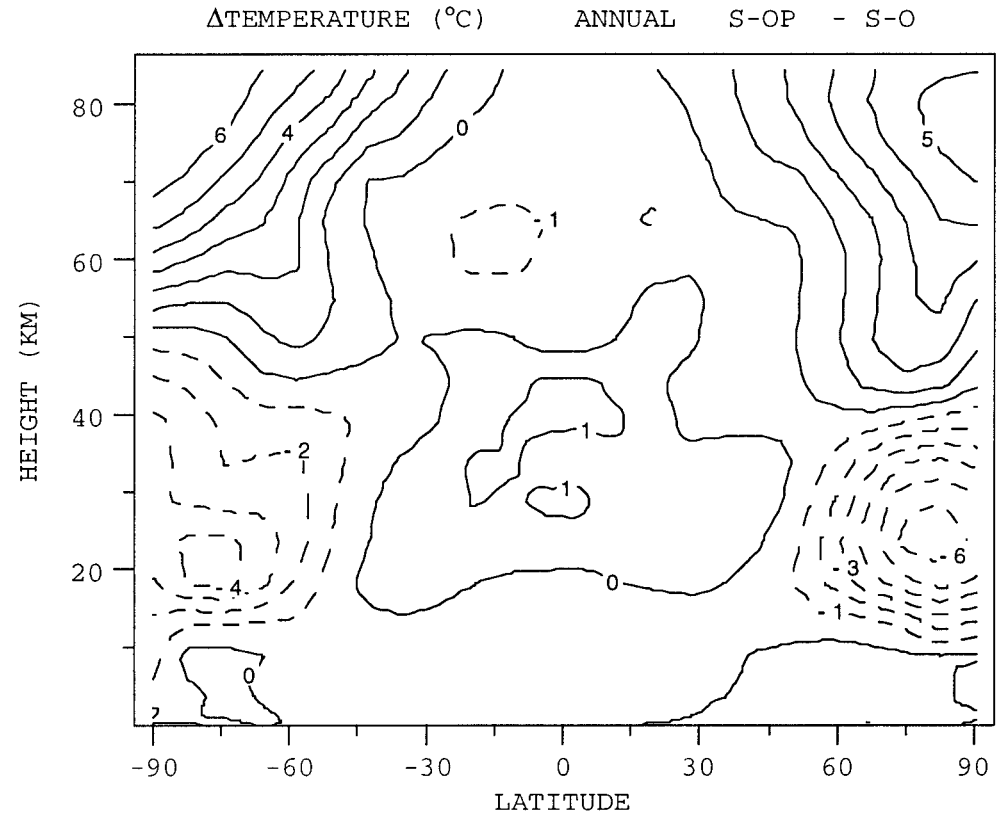
ΔTEMPERATURE (°C) ANNUAL S-OP - S-O
HEIGHT (KM)
80
60
40
20
-90
-60
-30
0
30
60
90
LATITUDE
6
4
0
5
-1
1
-2
1
1
0
-3
-6
-1
-4
0

cussed in paper 2. The fact that these changes do not strongly impact either tropospheric climate or stratospheric dynamics is understandable given the small magnitude of the tropospheric radiative forcing associated with the altered ozone. Since the tropospheric response in terms of both generation and propagation is basically the same, and since that essentially drives the stratospheric dynamical changes, little difference in the stratospheric eddy energy or residual circulation relative to the $2 \times CO_2$ simulation without ozone response would be expected.

Inclusion of PSC effects on ozone results in somewhat greater ozone reduction in the polar lower stratosphere and hence greater cooling there. The dynamical changes that arise from this influence are similar to the ozone hole effects simulated by Kiehl et al. (1988), Mahlman et al. (1994), and Wong and Rind (1998, submitted to *J. Atmos. Sci.*). In this case, including polar chemistry does influence some of the dynamical responses, since it affects wave energy propagating out of the troposphere; ideally the chemical changes should be done interactively with the dynamics. If chlorine levels do return to pre-1950 levels by the time doubled CO_2 equilibrium is reached, then the PSC effect is likely to be small.

7. Conclusions

The following are the main results of these experiments.

1) Allowing the sea surface temperatures to come into equilibrium with doubled CO_2 in the GCMAM results in 5.1°C warming.
2) In agreement with the results of paper 1, doubling CO_2 in both the stratosphere and troposphere leads to an increase in stratospheric eddy energy and residual circulation. The changes are large, on the order of 50%–70% for the annual average around 25-km altitude.
3) The tropical upper-tropospheric warming alters the refraction pattern for wave propagation into the stratosphere, helping to increase the EP flux convergences that drive the increased residual circulation.
4) The tropical warming also leads to a greater tropospheric zonal available potential energy, which ultimately results in larger long-wave energy in the troposphere; this appears to account for at least part of the stratospheric eddy kinetic energy increase.
5) These tropospheric and stratospheric energy changes do not occur in the GISS nine-level GCM with a top at 10 mb. The tropospheric changes require the increased vertical resolution in the troposphere, while the stratospheric response requires an elevated model top and better vertical resolution in the stratosphere.
6) Lifting the top to 0.68 mb (50 km) not only produces an accurate stratospheric change simulation, it also allows the upper troposphere–lower stratosphere stability, convection, and clouds to be calculated properly (compared to the GCMAM), which influences the climate sensitivity.
7) The increased long-wave energy in the GCMAM experiments is associated with increased eddy energy transports, while changes in condensational heat release produce different Hadley cell and mean circulation transports. These results emphasize that the differing energetic responses between the GCMAM and GCM affect many aspects of the simulated doubled CO_2 climate.
8) Stratospheric warmings decrease in the doubled CO_2 climate due to a reduction in wave 2 energy above 10 mb. Increased zonal winds in the middle stratosphere, associated with the tropical upper-troposphere warming, appear to retard the wave 2 energy propagation.
9) Ozone changes resulting from the doubled CO_2-induced stratospheric temperature changes reduce the upper-stratospheric cooling by about 20% (due to ozone increases) and cool the lower stratosphere slightly (due to ozone decreases).
10) The ozone response produces little net radiative forcing of the troposphere and thus little impact on surface air temperatures. It also does not significantly alter the stratospheric circulation response, which is driven by the troposphere.
11) Warming at low latitudes and cooling at high latitudes occur above the current tropopause locations due to doubled CO_2 temperature effects. Cooling in the polar lower stratosphere results in increased PSCs and ozone loss (with current chlorine levels), which leads to in situ cooling; its effect on the zonal wind structure modifies wave energy propagation, reducing the lower-stratospheric eddy energy gain

TABLE 6. Change in NH residual streamfunction in December–February due to doubled CO_2. Values are given in 10^7 kg s^{-1} and (%). Note that a negative value represents a strengthening of the existing circulation.

Experiment	23°N, 100 MB	39°N, 46 MB
S-C	−530 (53%)	−209 (44%)
S-S	−160 (18%)	−106.5 (24%)
H	−140 (16%)	+1 (−25%)
-M	−490 (41%)	−242 (49%)

←

FIG. 14. Annual zonal-averaged change in temperature due to doubled CO_2 and ozone response with polar stratospheric clouds (experiment minus its respective control run, indicated as control′) (top). Temperature difference between doubled CO_2 plus ozone response with and without polar stratospheric clouds (bottom).

and residual circulation increase, while increasing effects at higher altitudes.

Resolving the stratosphere and incorporating finer vertical resolution alters the model's dynamical and climate response to doubled CO_2 in both the troposphere and stratosphere. The optimum requirement for the position of the model top and vertical resolution are not yet certain, but it would appear as if many doubled CO_2 studies run with tops as low as 10 mb and nine vertical layers might well produce somewhat different results were they to incorporate finer vertical resolution and a fully resolved stratosphere. An increase in tropospheric vertical resolution in the boundary layer and upper troposphere had a noticeable impact on the dynamical results (and hence regional impacts associated with changes, for example, in the Hadley circulation). Raising the model top from 30 to 50 km allowed the stratospheric circulation changes to be resolved. Rind (1988) concluded from experiments with differing horizontal resolution that characteristics of the control run influenced the nature of the climate change results. These latest studies emphasize that variations in the vertical domain have an influence as well.

Acknowledgments. This work was supported by the NASA Chemistry Modeling and Analysis Program and the NASA EOS program; climate modeling at GISS is supported by the NASA Climate Modeling program.

REFERENCES

Austin, J., and N. Butchart, 1994: The influence of climate change and the timing of stratospheric warnings on arctic ozone depletion. *J. Geophys. Res.,* **99**, 1127–1145.

——, ——, and K. Shine, 1992: Possibility of an Arctic ozone hole in a doubled-CO_2 climate. *Nature,* **350,** 221–225.

Balachandran, N. K., and D. Rind, 1995: Modeling the effects of UV variability and the QBO on the troposphere–stratosphere system. Part I: The middle atmosphere. *J. Climate,* **8,** 2058–2079.

Boer, G. J., 1997: Some dynamical consequences of greenhouse gas warming. *Atmos.–Ocean,* **33,** 731–751.

Degorska, M., and B. Rajewska-Wiech, 1996: The role of minor stratospheric warmings in producing the total ozone deficiencies over Europe in 1992 and 1993. *J. Atmos. Terr. Phys.,* **58,** 1855–1862.

Hansen, J. E., G. Russell, D. Rind, P. Stone, A. Lacis, S. Lebedeff, R. Ruedy, and L. Travis, 1983: Efficient three-dimensional global models for climate studies: Models I and II. *Mon. Wea. Rev.,* **111,** 609–662.

——, and Coauthors, 1984: Climate sensitivity: Analysis of feedback mechanisms. *Climate Processes and Climate Sensitivity, Geophysical Monogr. 29,* Amer. Geophys. Union, 130–163.

——, M. Sato, and R. Ruedy, 1997: Radiative forcing and climate response. *J. Geophys. Res.,* **102,** 6831–6864.

IPCC, 1992: *Climate Change 1992*. J. T. Houghton, B. A. Callander, and S. K. Varney, Eds., Cambridge University Press, 93 pp.

——, 1996: *Climate Change 1995*. J. T. Houghton, L. G. Meira Filho, B. A. Callander, N. Harris, A. Kattenberg, and K. Maskell, Eds., Cambridge University Press, 572 pp.

Kao, S.-K., and J. F. Sagendorf, 1970: The large-scale meridional transport of sensible heat in wavenumber frequency space. *Tellus,* **22,** 172–185.

Kiehl, T., B. A. Boville, and B. P. Briegleb, 1988: Response of a general circulation model to a prescribed Antarctic ozone hole. *Nature,* **332,** 501–504.

Kodera, K., 1994: Influence of volcanic eruptions on the troposphere through stratospheric dynamical process in the Northern Hemisphere winter. *J. Geophys. Res.,* **99,** 1273–1282.

——, and M. Chiba, 1995: Tropospheric circulation changes associated with stratospheric sudden warmings: A case study. *J. Geophys. Res.,* **100,** 11 055–11 068.

Lacis, A. A., D. J. Wuebbles, and J. A. Logan, 1990: Radiative forcing of climate by changes in the vertical distribution of ozone. *J. Geophys. Res.,* **95,** 9971–9981.

London, J., 1963: Ozone variations and their relation to stratospheric warmings. *Symposium on Stratospheric and Mesospheric Circulation,* Vol. 36, *Meteorologische Abhandlungen der Freien Universität Berlin,* 299–310.

Mahfouf, J. F., D. Cariolle, J.-F. Royer, J.-F. Geleyn, and B. Timbal, 1994: Response of the Meteo-France climate model to changes in CO_2 and sea surface temperature. *Climate Dyn.,* **9,** 345–362.

Mahlman, J. D., J. P. Pinto, and L. J. Umscheid, 1994: Transport, radiative and dynamical effects of the Antarctic ozone hole: A GFDL ''SKYHI'' model experiment. *J. Atmos. Sci.,* **51,** 489–508.

O'Neill, A., and V. D. Pope, 1988: Simulation of linear and nonlinear disturbances in the stratosphere. *Quart. J. Roy. Meteor. Soc.,* **114,** 1063–1075.

Phillips, T. J., 1994: A summary documentation of the AMIP models. PCMDI Rep. No. 18, Lawrence Livermore National Laboratory, 343 pp. [Available from U.S. Dept. of Commerce, 5285 Port Royal Rd., Springfield, VA 22161.]

Rind, D., 1988: Dependence of warm and cold climate depiction on climate model resolution. *J. Climate,* **1,** 965–997.

——, and N. K. Balachandran, 1995: Modeling the effects of UV variability and the QBO on the troposphere–stratosphere system. Part II: The troposphere. *J. Climate,* **8,** 2080–2095.

——, and P. Lonergan, 1995: Modeled impacts of stratospheric ozone and water vapor perturbations with implications for high-speed civil transport aircraft. *J. Geophys. Res.,* **100,** 7381–7396.

——, and J. Lerner, 1996: The use of on-line tracers as a diagnostic tool in GCM model development. *J. Geophys. Res.,* **101,** 12 667–12 683.

——, R. Suozzo, N. K. Balachandran, A. Lacis, and G. Russell, 1988a: The GISS global climate/middle atmosphere model. Part I: Model structure and climatology. *J. Atmos. Sci.,* **45,** 329–370.

——, ——, and ——, 1988b: The GISS global climate/middle atmosphere model. Part II: Model variability due to interactions between planetary waves, the mean circulation and gravity wave drag. *J. Atmos. Sci.,* **45,** 371–386.

——, ——, ——, and M. J. Prather, 1990: Climate change and the middle atmosphere. Part I: The doubled CO_2 climate. *J. Atmos. Sci.,* **47,** 475–494.

——, ——, and ——, 1992: Climate change and the middle atmosphere. Part II: The impact of volcanic aerosols. *J. Climate,* **5,** 189–208.

——, R. Healy, C. Parkinson, and D. Martinson, 1995: The role of sea ice in $2 \times CO_2$ climate model sensitivity. Part I: The total influence of sea ice thickness and extent. *J. Climate,* **8,** 448–463.

Shindell, D. T., D. Rind, and P. Lonergan, 1998: Climate change and the middle atmosphere. Part IV: Ozone response to doubled CO_2. *J. Climate,* **11,** 895–918.

Zullig, W., 1973: Relation between the intensity of the stratospheric circumpolar vortex and the accumulation of ozone in the winter hemisphere. *Pure Appl. Geophys.,* **106–108,** 1544–1552.